Reabsorption of Soft X-Ray Emission at High X-Ray Free-Electron Laser Fluences

Simon Schreck, Martin Beye, Jonas A. Sellberg, Trevor McQueen, Hartawan Laksmono, Brian Kennedy, Sebastian Eckert, Daniel Schlesinger, Dennis Nordlund, Hirohito Ogasawara, Raymond G. Sierra, Vegard H. Segtnan, Katharina Kubicek, William F. Schlotter, Georgi L. Dakovski, Stefan P. Moeller, Uwe Bergmann, Simone Techert, Lars G. M. Pettersson, Philippe Wernet, Michael J. Bogan, Yoshihisa Harada, Anders Nilsson, and Alexander Föhlisch

Reabsorption of Soft X-ray Emission at High X-ray Free-Electron Laser Fluences

Simon Schreck,[1, 2, *] Martin Beye,[1, †] Jonas A. Sellberg,[3, 4] Trevor McQueen,[4, 5] Hartawan Laksmono,[6]
Brian Kennedy,[1] Sebastian Eckert,[1] Daniel Schlesinger,[3] Dennis Nordlund,[7] Hirohito Ogasawara,[7]
Raymond G. Sierra,[6] Vegard H. Segtnan,[4, 8] Katharina Kubicek,[9, 10] William F. Schlotter,[11] Georgi L. Dakovski,[11]
Stefan P. Moeller,[11] Uwe Bergmann,[11] Simone Techert,[9, 10, 12] Lars G. M. Pettersson,[3] Philippe Wernet,[1]
Michael J. Bogan,[6] Yoshihisa Harada,[13, 14] Anders Nilsson,[3, 4, 7] and Alexander Föhlisch[1, 2]

[1]*Institute for Methods and Instrumentation in Synchrotron Radiation Research,*
Helmholtz-Zentrum Berlin für Materialien und Energie GmbH,
Albert-Einstein-Str. 15, 12489 Berlin, Germany
[2]*Institut für Physik und Astronomie, Universität Potsdam,*
Karl-Liebknecht-Strasse 24-25, 14476 Potsdam, Germany
[3]*Department of Physics, AlbaNova University Center,*
Stockholm University, S-106 91 Stockholm, Sweden
[4]*SUNCAT, SLAC National Accelerator Laboratory,*
2575 Sand Hill Road, Menlo Park, California 94025, USA
[5]*Department of Chemistry, Stanford University, Stanford, CA 94305, USA*
[6]*PULSE Institute, SLAC National Accelerator Laboratory,*
2575 Sand Hill Road, Menlo Park, California 94025, USA
[7]*SSRL, SLAC National Accelerator Laboratory, 2575 Sand Hill Road, Menlo Park, California 94025, USA*
[8]*Nofima AS, Osloveien 1, N-1430 Ås, Norway*
[9]*FS-Structural Dynamics in (Bio)chemistry, Deutsches Elektronen-Synchrotron, Notkestrasse 85, 22607 Hamburg, Germany*
[10]*Max Planck Institute for Biophysical Chemistry, Am Faßberg 11, 37077 Göttingen, Germany*
[11]*LCLS, SLAC National Accelerator Laboratory, 2575 Sand Hill Road, Menlo Park, California 94025, USA*
[12]*Institute for X-ray Physics, Georg-August-Universität Göttingen,*
Friedrich-Hund-Platz 1, 37077 Göttingen, Germany
[13]*Institute for Solid State Physics (ISSP), University of Tokyo, Kashiwanoha, Kashiwa, Chiba 277-8581, Japan*
[14]*Synchrotron Radiation Research Organization, University of Tokyo, Sayo-cho, Sayo, Hyogo 679-5198, Japan*
(Dated: July 9, 2014)

We report on oxygen K-edge soft x-ray emission spectroscopy from a liquid water jet at the Linac Coherent Light Source. We observe significant changes in the spectral content when tuning over a wide range of incident x-ray fluences. At high fluences, also the total emission yield decreases. These modifications result from reabsorption of x-ray emission by valence-excited molecules generated by the Auger cascade. Our observations have major implications for future x-ray emission studies at intense x-ray sources. We highlight the importance of the x-ray pulse length with respect to the core-hole lifetime.

The ultrahigh peak brilliances available at x-ray free electron lasers (XFELs) enable experimentalists to explore new regimes of light-matter interaction. Non-linear spectroscopies, which are well established for optical wavelengths (e.g. stimulated Raman scattering), have been proposed [1–3] and recently pioneered in the soft x-ray regime [4–6]. In particular, stimulated effects in x-ray emission (XE) and resonant inelastic x-ray scattering (RIXS) promise to improve signal levels by orders of magnitude. This will enable an efficient application of these highly selective spectroscopies to study elementary low-energy excitations in e.g. physical chemistry and materials science [7–10].

However, the required high photon densities generate significant concurrent radiation damage as a result of Auger decays and subsequent electron cascades. In the limit of complete stimulation, this damaging non-radiative decay channel should be fully switched off by stimulating the radiative decay faster than the Auger-dominated natural core-hole lifetime [5]. But in an intermediate regime, the electron cascades will prevent prob-

ing of the undisturbed system. We present here the fundamental processes during the transition from the linear single-photon to the non-linear multi-photon regime in soft x-ray-matter interaction. Their complete understanding is essential to fully exploit the potential of stimulated as well as normal XE spectroscopy at XFELs.

We report on soft XE spectroscopy from a liquid water jet for a wide range of incident x-ray fluences at the Linac Coherent Light Source (LCLS) at the SLAC National Accelerator Laboratory. For fluences exceeding the linear single-photon regime (above $\approx 0.2\,\mathrm{J/cm^2}$ in this work) we observe significant modifications of the spectra as well as a decrease of the total emission yield. These modifications are interpreted as a result of reabsorption of the emitted x-rays by valence-excited molecules. The valence excitations are generated by the ultrafast Auger cascade. Based on this mechanism, we present a model that describes the measured data through the single-photon regime and up to $\approx 10\,\mathrm{J/cm^2}$ for the conditions in this work.

We performed experiments at the soft x-ray materials

science instrument (SXR) of the LCLS [11]. To measure oxygen K-edge XE spectra from liquid water we used the Liquid Jet Endstation (LJE) [12, 13]. Briefly, the LJE features a 20 μm diameter liquid microjet in vacuum and a Grace spectrometer XES 350 [14] mounted at 90° with respect to the incident x-ray beam (inset of Figure 1). The sample volume in the interaction region is exchanged with a kHz − MHz repetition rate by the liquid jet (depending on flow rate, jet diameter and vertical x-ray spot size). Therefore each x-ray pulse, arriving with a repetition rate of 120 Hz, probes a new liquid water sample. We used the unmonochromatized beam with a central photon energy of 550 eV (well above the oxygen K-edge absorption resonance) with a bandwidth of ≈ 5 eV from 100 fs (full width at half maximum, FWHM) long electron bunches. The x-ray spot size was varied using the bendable Kirkpatrick-Baez (KB) focusing optics of the SXR instrument. Four different spot sizes were used (hor.×vert.): $25 \times 20 \,\mu m^2$, $20 \times 70 \,\mu m^2$, $35 \times 170 \,\mu m^2$ and $75 \times 520 \,\mu m^2$ (FWHM, determined by microscope images of a fluorescent screen [15]). In addition the gas attenuator was scanned for each spot size, which enabled a continuous variation of the incident x-ray fluence at the sample between 0.01 and 20 J/cm². Scans at different spot sizes were properly normalized to account for different illuminated areas as well as changes in the experimental alignment [15]. The x-ray pulse energy was measured with a shot-to-shot pulse energy monitor [16–18] located in the front end upstream of the entire SXR beamline. The number of photons per pulse at the sample were calculated by assuming 10% x-ray transmission from this front end pulse energy monitor to the sample as determined from commissioning results of a further pulse energy monitor located downstream in the SXR beamline (just upstream of the KB optics). Reference spectra were measured with the same setup at beamline U49/2 PGM-1 of the synchrotron radiation source BESSY II at the Helmholtz-Zentrum Berlin, Germany.

We illustrate the experimental arrangement in the inset of Figure 1. The red shaded volume represents the excited volume where the incident x-rays interact with the liquid water sample. Since the penetration depth (0.5 μm [19]) of 550 eV x-rays in water is significantly shorter than the dimensions of the x-ray spot, the excited volume forms a thin curved sheet on the liquid jet surface.

In Figure 1 we present the complete experimental data set. The detected x-ray emission yield (emission signal divided by incident fluence) is shown as a function of emission energy and incident fluence. Note the logarithmic scale of the fluence axis. Increasing x-ray fluence results in a significant decrease of the emission yield. This decrease is nonuniform for different emission energies, which results in spectral distortions. We observed at most 80 counts in a single-shot image and can thus exclude saturation effects in the detection system.
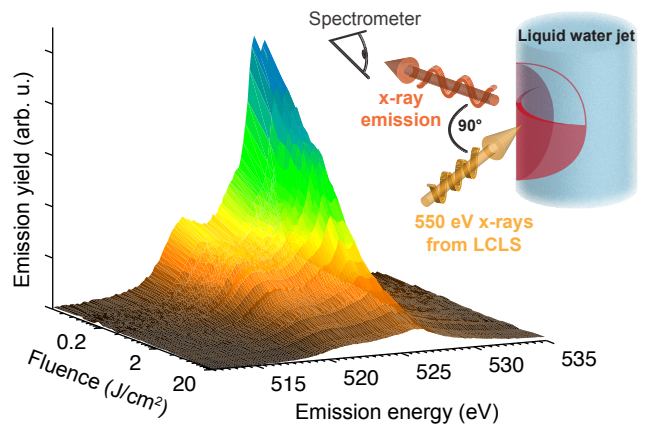

FIG. 1. X-ray emission spectra for a wide range of incident x-ray fluences. The lower emission yield and distortion of the spectra with increasing fluence are observed. The inset shows a schematic illustration of the experimental arrangement. The red shaded volume represents the excited volume for an x-ray spot size of about $20 \times 20 \,\mu m^2$.

To quantify these experimental findings, we display in Figure 2(a) how the integrated emission signal changes with the incident fluence. We observe the expected linear dependence of incident and detected photon numbers only for the low fluence regime up to ≈ 0.2 J/cm² (lower inset). For higher fluences the detected emission signal rises less than linearly with a square root like dependence. From about 10 J/cm² a linear dependence sets in again, however, with a smaller slope than in the low fluence regime. In Figure 2(b) we analyze the spectral distortions. We compare XE spectra for selected fluences from LCLS with a reference spectrum from BESSY II. The lowest fluence LCLS spectrum agrees well with the reference spectrum from BESSY II as well as with previous XE studies of liquid water at other synchrotron light sources [20, 21]. For increasing fluence the most intense emission feature (around 526 eV emission energy) starts to decrease in intensity first. For even higher fluences also the less intense regions of the spectrum decrease in intensity.

To understand this non-linearity in the detected emission intensity and the spectral distortion, we depict in Figure 3(a) the two major decay channels after absorption of a 550 eV photon. The absorption removes an electron from the oxygen 1s core-level and leaves the molecule in a core-ionized state. This state has a lifetime of about 4 fs [22]. The dominant decay channel in the soft x-ray regime (> 99% [23]) is non-radiative Auger decay. Here an electron from the occupied valence levels fills the core-hole. The excess energy is transferred to a second electron (Auger electron) from the valence levels, which leaves the molecule with a kinetic energy of about 500 eV [24]. The Auger electron then scatters elastically as well as inelastically at surrounding water molecules
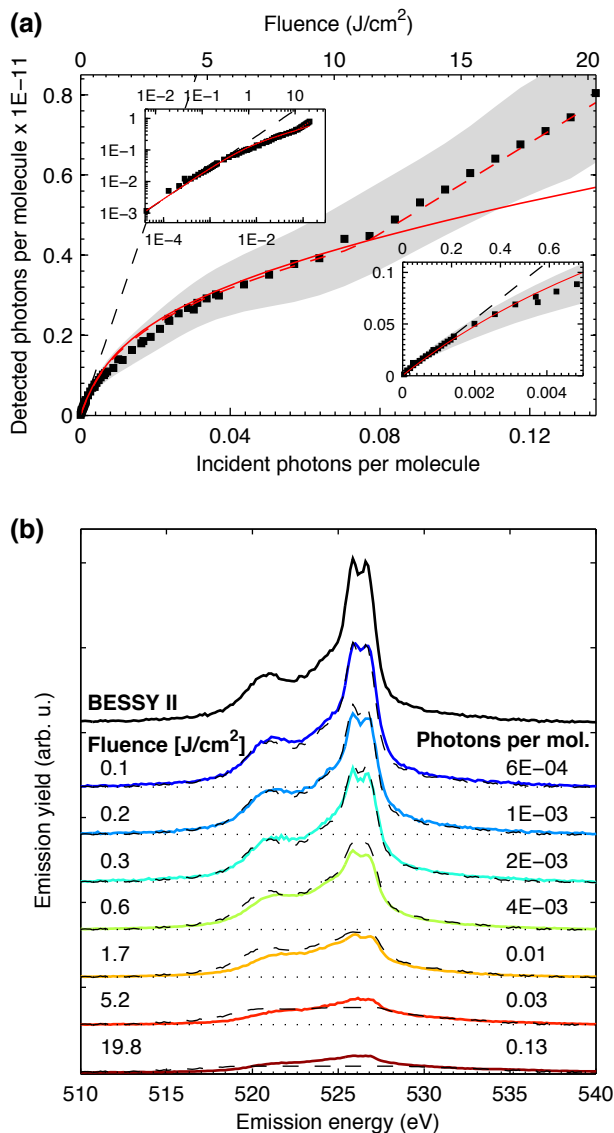
(a)

(b)

FIG. 2. (a) Detected signal as a function of incident photon numbers. Markers represent measured data and the grey shaded area gives a 1σ confidence band representing the measurement uncertainties. Red curves (solid and dashed) are results of the model described in the main text. Dashed black line is a linear fit to the experimental data below $0.2\,\mathrm{J/cm^2}$. The lower right inset gives a zoom into the low fluence regime. The upper left inset shows the complete data set on a double logarithmic scale. (b) X-ray emission spectra from BESSY II (solid black curve) and for selected incident fluences at LCLS (colored curves). The dashed black curve superimposed with each LCLS spectrum is the result of the model described in the main text.
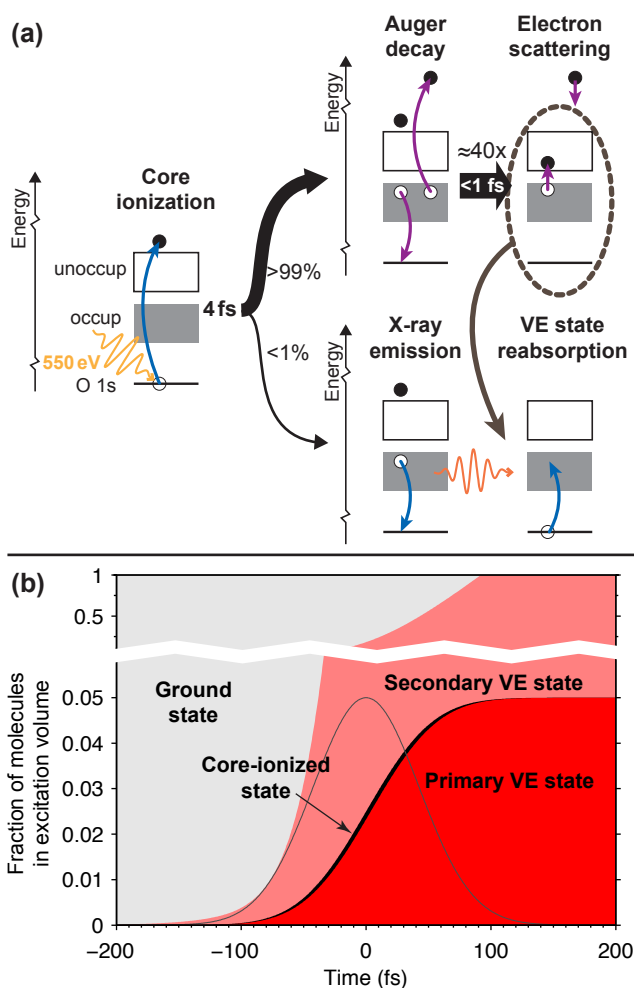
(a)

(b)

FIG. 3. Processes after oxygen $1s$ core ionization: (a) The dominating non-radiative Auger decay channel (top) leaves the molecule in a double valence hole state. The emitted fast electron can create about forty secondary valence-excited states on the timescale of a few femtoseconds through electron scattering. The photons from a radiative decay (bottom) can, at high excitation densities, get reabsorbed by valence-excited molecules. (b) Exemplary time-evolution of the different states of the molecules in the excited volume. The experimental parameters for $7\,\mathrm{J/cm^2}$ in a single gaussian XFEL pulse of $100\,\mathrm{fs}$ duration (grey line) are applied. Since a single Auger decay can create about forty secondary valence-excited states, the respective fraction of molecules increases quickly and becomes significant far before the pulse reaches its maximum. The majority of decays from the core-ionized state happens in the presence of significant valence excitations. - VE = valence-excited.

(Auger cascade). In each inelastic scattering event a portion of the electron kinetic energy is transferred to a water molecule ultimately creating a valence-excitation in this molecule. A single primary Auger electron can create tens of valence excitations within a few femtoseconds [25–29].

The detected XE photons result from the radiative decay of the core-ionized molecule (Figure 3(a), bottom). These photons have an energy below the core-level absorption resonance. Hence the probability for absorption by surrounding molecules in the ground state is low. The relevant valence orbitals for core to valence transitions are occupied. However, molecules in a valence-excited

state can absorb the photon, as they have a hole in the corresponding valence levels. An emitted x-ray photon can get reabsorbed by a molecule that has a valence hole at exactly the same level that the photon was emitted from. We show in the following that this reabsorption of x-ray emission by valence-excited molecules within a single XFEL pulse is responsible for the decrease in total emission yield as well as for the spectral distortions.

During data analysis we considered alternative mechanisms to explain our observations. In particular stimulated x-ray emission could focus the radiative decay [5] into a direction outside the spectrometer acceptance and hence decrease the emission yield detected in the spectrometer. However, due to the long XFEL pulse (100 fs) as compared to the oxygen 1s core-hole life time (4 fs) the high core-hole density needed for stimulated emission is not achieved in our experiment (see below and Figure 3(b)). Using the formalism from Beye et al. [5], we expect stimulated emission to become sizable only around $1000 \, \text{J/cm}^2$ in our case. This mechanism should furthermore cause the same decrease of emission yield for all emission energies in contrast to our observations. Other possible non-linear effects like power-broadening, multiphoton absorption, harmonic generation and saturated x-ray absorption also struggle to explain the spectral distortions.

For a quantitative description of the data the valence hole density ρ_{vh} is a central quantity, since it determines the probability for reabsorption. ρ_{vh} increases with increasing fluence and can get bigger than the density of molecules, since each molecule can have multiple valence holes. We assume ρ_{vh} to develop much faster than the incoming x-ray pulse, i.e. we ignore the temporal evolution of the excitations in the sample during the XFEL pulse.

This approach is justified through a comparison of the relevant timescales, Figure 3(b). We illustrate the time-evolution of the excited molecules during the 100 fs XFEL pulse. We assume a gaussian envelope for the temporal intensity distribution in the pulse. Each incident photon creates a core-ionized molecule, which decays within the core-hole lifetime of 4 fs [22] (for the oxygen K-edge) into a valence-ionized state. Hence only a small fraction of molecules in the excited volume is core-ionized at each time point within the XFEL pulse. This fraction of core-ionized molecules is represented by the black area in Figure 3(b). After the Auger decay, the originally core-ionized molecules are in a doubly valence-ionized state, that we call the primary valence-excited state and represent by the dark red area in Figure 3(b). This state has a lifetime significantly longer than the XFEL pulse length. The emitted energetic Auger electron scatters at other primarily unexcited molecules (Auger cascade) and looses its energy by creating valence-excitations in these molecules. These we call here secondary valence-excited states and represent them by the light red area in

Figure 3(b). We conservatively assumed a 10 fs [28] duration for the Auger cascade and 40 secondary valence-excitations from a single Auger electron. The rapid increase of valence-excited molecules already in the early part of the XFEL pulse justifies neglecting the time evolution of the valence hole density.

For a proper description of the valence hole density as a function of incident intensity (see [15] for a detailed derivation) we consider the minimum energy needed to create one valence hole E_{vh}. For the first valence hole in a molecule E_{vh} equals the band gap E_{HL} while it increases stepwise for each additional valence hole to be created in the molecule. However, the average of E_{vh} over the ensemble of molecules in the excited volume will increase linearly from E_{HL} up to $E_{\text{HL}} + 2\,E_{\text{BW}}$ with E_{BW} being the bandwidth of the valence band. The total energy needed to create ρ_{vh} valence holes per molecule follows from integrating E_{vh} up to ρ_{vh}. From the result of this integration we derive an expression for ρ_{vh} as a function of the total energy E_{tot} that was deposited in each molecule in the excited volume. E_{tot} is directly connected to the number of incident photons N_{in} and the number density of molecules n_{mol}: $E_{\text{tot}} = (N_{\text{in}} \, h\nu)/n_{\text{mol}}$. Finally we find a square root dependence of ρ_{vh} on the number of incident photons with material constants a and b:

$$\rho_{\text{vh}} = -a + \sqrt{a^2 + b \cdot N_{\text{in}}}. \tag{1}$$

At this point equation (1) gives the number of valence holes per molecule. To obtain the valence hole density we multiply by n_{mol}.

From a simple rate equation (see [15] for the explicit formulation) we derive an expression for the number of detected photons as function of incident intensity and emission energy. We fit this expression to the experimental data with a single free parameter that accounts for the overall signal strength, including e.g. detection efficiency and the quality of the experimental alignment. All other parameters in the model are determined by the experimental geometry or are properties of the studied material.

The fitted curves are presented together with the experimental data in Figure 2. We find good agreement with the integrated emission intensity (Figure 2(a), solid red curve) up to an incident fluence of about $10 \, \text{J/cm}^2$, including the linear dependence in the low fluence regime and the following non-linearity due to the onset of reabsorption. The second linear dependence above $10 \, \text{J/cm}^2$ is not reproduced by our model.

We model the spectral distortions with the same parameter set (Figure 2(b)). The general trend of stronger intensity decrease for the more intense emission lines due to a higher valence hole density for the corresponding valence levels [15] is reproduced. While the model describes the measured data well at lower fluences, we observe again deviations at the upper end of the studied fluence range.

The fundamental reason for the observed deviations from our model at extremely high fluences above $10 \, \text{J/cm}^2$ lies in our application of ground state parameters. We use the electronic structure and the cross-sections from the low fluence regime, where those properties are determined by the ground state. In the high fluence regime the studied system considerably deviates from the ground state and our model anticipates water molecules with far more than one valence hole. Effects like Coulomb explosion strongly affecting the geometric structure have been observed for heavier elements e.g. silicon [30–34] in a similar fluence regime and have been predicted and observed for lighter elements at significantly higher fluences [35, 36]. Although a detailed description of the connected effects on the electronic structure and nuclear motions is beyond the scope of this paper, the created valence holes can still reabsorb x-ray emission at these high fluences. In general, we anticipate a lower probability for the creation of additional valence holes and smaller interaction cross-sections due to the lowered number of electrons in the valence levels at high fluences. These changes would lead to smaller reabsorption effects than predicted with our model, which agrees with the observed evolution.

We can empirically include these effects through introducing an upper limit for the valence hole density of 2.8 holes per molecule, resulting in the dashed red curve in Figure 2(a), which matches the measured data. For a full theoretical description, simulations of the complete Auger cascade including the time evolution of the core- and valence-excited states are necessary, including possible multiple excitations. These simulations have been performed for different materials and parameter spaces including water and ice [26–29], while they mostly concentrated on much lower fluence ranges.

In summary the derived model provides a satisfactory description of the experimental data. We have presented strong evidence that ultrafast generation of a multitude of valence holes within a single intense XFEL pulse and the following reabsorption of x-ray emission by valence-excited molecules are responsible for significant spectral distortions and a decrease in the detected emission yield.

Our findings have important implications for future XE and RIXS studies at XFEL sources. Since the presented reabsorption mechanism is mostly independent of the studied material measurements from dense samples at high fluences will effectively always result in high valence hole densities and hence be accompanied by additional effects, like reabsorption and spectral distortions. Approaches to prevent these high valence hole densities while still using the ultrahigh peak brilliance available at XFELs are desirable and could be realized through completely stimulating radiative decays and thus preventing electronically damaging Auger decays [5].

In addition we stress the importance of short XFEL pulses. A high instantaneous core-hole density and simultaneously a low valence-hole density are required for stimulated XE without reabsorption. This can only be achieved with an XFEL pulse length on the order of or shorter than the core-hole lifetime. Longer XFEL pulses will always lead to a high density of secondary valence excited-states and prevent probing of the undisturbed system.

---

[*] simon.schreck@helmholtz-berlin.de

[†] martin.beye@helmholtz-berlin.de

[1] S. Tanaka and S. Mukamel, Phys. Rev. Lett. **89**, 043001 (2002).

[2] N. Rohringer and R. Santra, Phys. Rev. A **76**, 033416 (2007).

[3] B. D. Patterson, "Resource letter on stimulated inelastic x-ray scattering at an XFEL." SLAC Technical Note SLAC-TN-10-026, SLAC National Accelerator Laboratory, Menlo Park, California (2010).

[4] N. Rohringer, D. Ryan, R. A. London, M. Purvis, F. Albert, J. Dunn, J. D. Bozek, C. Bostedt, A. Graf, R. Hill, S. P. Hau-Riege, and J. J. Rocca, Nature **481**, 488 (2012).

[5] M. Beye, S. Schreck, F. Sorgenfrei, C. Trabant, N. Pontius, C. Schüßler-Langeheine, W. Wurth, and A. Föhlisch, Nature **501**, 191 (2013).

[6] C. Weninger, M. Purvis, D. Ryan, R. A. London, J. D. Bozek, C. Bostedt, A. Graf, G. Brown, J. J. Rocca, and

N. Rohringer, Phys. Rev. Lett. **111**, 233902 (2013).

[7] A. Kotani and S. Shin, Rev. Mod. Phys. **73**, 203 (2001).

[8] L. J. P. Ament, M. van Veenendaal, T. P. Devereaux, J. P. Hill, and J. van den Brink, Rev. Mod. Phys. **83**, 705 (2011).

[9] J.-E. Rubensson, A. Pietzsch, and F. Hennies, J. El. Spec. Rel. Phen. **185**, 294 (2012).

[10] J.-E. Rubensson, F. Hennies, and A. Pietzsch, J. El. Spec. Rel. Phen. **188**, 79 (2013).

[11] W. F. Schlotter, J. J. Turner, M. Rowen, P. Heimann, M. Holmes, O. Krupin, M. Messerschmidt, S. Moeller, J. Krzywinski, R. Soufli, M. Fernández-Perea, N. Kelez, S. Lee, R. Coffee, G. Hays, M. Beye, N. Gerken, F. Sorgenfrei, S. Hau-Riege, L. Juha, J. Chalupsky, V. Hajkova, A. P. Mancuso, A. Singer, O. Yefanov, I. A. Vartanyants, G. Cadenazzi, B. Abbey, K. A. Nugent, H. Sinn, J. Lüning, S. Schaffert, S. Eisebitt, W.-S. Lee, A. Scherz, A. R. Nilsson, and W. Wurth, Rev. Sci. Instrum. **83**, 043107 (2012).

[12] K. Kunnus, I. Rajkovic, S. Schreck, W. Quevedo, S. Eckert, M. Beye, E. Suljoti, C. Weniger, C. Kalus, S. Grübel, M. Scholz, D. Nordlund, W. Zhang, R. W. Hartsock, K. J. Gaffney, W. F. Schlotter, J. J. Turner, B. Kennedy, F. Hennies, S. Techert, P. Wernet, and A. Föhlisch, Rev. Sci. Instrum. **83**, 123109 (2012).

[13] I. Rajkovic, J. Hallmann, S. Grübel, R. More, W. Quevedo, M. Petri, and S. Techert, Rev. Sci. Instrum. **81**, 045105 (2010).

[14] J. Nordgren, G. Bray, S. Cramm, R. Nyholm, J.-E. Rubensson, and N. Wassdahl, Rev. Sci. Instrum. **60**, 1690 (1989).

[15] See Supplemental Material at [URL will be inserted by publisher] for details on the calibration of the incident x-ray fluence, the explicit derivation of the described model, the used parameters.

[16] S. P. Hau-Riege, R. M. Bionta, D. D. Ryutov, and J. Krzywinski, J. Appl. Phys. **103**, 053306 (2008).

[17] S. P. Hau-Riege, R. M. Bionta, D. D. Ryutov, R. A. London, E. Ables, K. I. Kishiyama, S. Shen, M. A. McKernan, D. H. McMahon, M. Messerschmidt, J. Krzywinski, P. Stefan, J. Turner, and B. Ziaja, Phys. Rev. Lett. **105**, 043003 (2010).

[18] S. Moeller, J. Arthur, A. Brachmann, R. Coffee, F. J. Decker, Y. Ding, D. Dowell, S. Edstrom, P. Emma, Y. Feng, A. S. Fisher, J. Frisch, J. Galayda, S. Gilevich, J. Hastings, G. Hays, P. Hering, Z. Huang, R. Iverson, J. Krzywinski, S. Lewis, H. Loos, M. Messerschmidt, A. Miahnahri, H. D. Nuhn, D. Ratner, J. Rzepiela, D. Schultz, T. Smith, P. Stefan, H. Tompkins, J. Turner, J. Welch, B. White, J. Wu, G. Yocky, R. Bionta, E. Ables, B. Abraham, C. Gardener, K. Fong, S. Friedrich, S. P. Hau-Riege, K. Kishiyama, T. McCarville, D. McMahon, M. McKernan, L. Ott, M. Pivovaroff, J. Robinson, D. Ryutov, S. Shen, R. Soufli, and G. Pile, Nucl. Instrum. & Methods in Phys. Research Section A **635**, S6 (2011).

[19] B. L. Henke, E. Gullikson, and J. C. Davis, At. Data Nucl. Data Tables **54**, 181 (1993).

[20] T. Tokushima, Y. Harada, O. Takahashi, Y. Senba, H. Ohashi, L. G. M. Pettersson, A. Nilsson, and S. Shin, Chem. Phys. Lett. **460**, 387 (2008).

[21] O. Fuchs, M. Zharnikov, L. Weinhardt, M. Blum, M. Weigand, Y. Zubavichus, M. Bär, F. Maier, J. D. Denlinger, C. Heske, M. Grunze, and E. Umbach, Phys. Rev. Lett. **100**, 027801 (2008).

[22] F. Gel'mukhanov, H. Ågren, M. Neeb, J.-E. Rubensson, and A. Bringer, Phys. Lett. A **211**, 101 (1996).

[23] J. H. Hubbell, P. N. Trehan, N. Singh, B. Chand, D. Mehta, M. L. Garg, R. R. Garg, S. Singh, and S. Puri, J. Phys. Chem. Ref. Data **23**, 339 (1994).

[24] D. Nordlund, H. Ogasawara, H. Bluhm, O. Takahashi, M. Odelius, M. Nagasono, L. G. M. Pettersson, and A. Nilsson, Phys. Rev. Lett. **99**, 217406 (2007).

[25] W. Werner, Surf. and Interf. Analysis **31**, 141 (2001).

[26] B. Ziaja, D. van der Spoel, A. Szöke, and J. Hajdu, Phys. Rev. B **64**, 214104 (2001).

[27] B. Ziaja, A. Szöke, D. van der Spoel, and J. Hajdu, Phys. Rev. B **66**, 024116 (2002).

[28] N. Tîmneanu, C. Caleman, J. Hajdu, and D. van der Spoel, Chem. Phys. **299**, 277 (2004).

[29] N. Medvedev, H. O. Jeschke, and B. Ziaja, New J. Phys. **15**, 015016 (2013).

[30] A. Rousse, C. Rischel, S. Fourmaux, I. Uschmann, S. Sebban, G. Grillon, P. Balcou, E. Förster, J. P. Geindre, P. Audebert, J. C. Gauthier, and D. Hulin, Nature **410**, 65 (2001).

[31] N. Stojanovic, D. von der Linde, K. Sokolowski-Tinten, U. Zastrau, F. Perner, E. Forster, R. Sobierajski, R. Nietubyc, M. Jurek, D. Klinger, J. Pelka, J. Krzywinski, L. Juha, J. Cihelka, A. Velyhan, S. Koptyaev, V. Hajkova, J. Chalupsky, J. Kuba, T. Tschentscher, S. Toleikis, S. Dusterer, and H. Redlin, Appl. Phys. Lett. **89**, 241909 (2006).

[32] S. P. Hau-Riege, R. A. London, R. M. Bionta, M. A. McKernan, S. L. Baker, J. Krzywinski, R. Sobierajski, R. Nietubyc, J. B. Pelka, M. Jurek, L. Juha, J. Chalupsky, J. Cihelka, V. Hajkova, A. Velyhan, J. Krasa, J. Kuba, K. Tiedtke, S. Toleikis, T. Tschentscher, H. Wabnitz, M. Bergh, C. Caleman, K. Sokolowski-Tinten, N. Stojanovic, and U. Zastrau, Appl. Phys. Lett. **90**, 173128 (2007).

[33] R. Sobierajski, D. Klinger, M. Jurek, J. B. Pelka, L. Juha, J. Chalupsk, J. Cihelka, V. Hakova, L. Vysin, U. Jastrow, N. Stojanovic, S. Toleikis, H. Wabnitz, J. Krzywinski, S. Hau-Reige, and R. London, Proc. SPIE 7361, Damage to VUV, EUV, and X-Ray Optics II , 736107 (2009).

[34] T. Koyama, H. Yumoto, Y. Senba, K. Tono, T. Sato, T. Togashi, Y. Inubushi, T. Katayama, J. Kim, S. Matsuyama, H. Mimura, M. Yabashi, K. Yamauchi, H. Ohashi, and T. Ishikawa, Opt. Express **21**, 15382 (2013).

[35] M. Bergh, N. Tîmneanu, and D. van der Spoel, Phys. Rev. E **70**, 051904 (2004).

[36] B. F. Murphy, T. Osipov, Z. Jurek, L. Fang, S.-K. Son, M. Mucke, J. H. D. Eland, V. Zhaunerchyk, R. Feifel, L. Avaldi, P. Bolognesi, C. Bostedt, J. D. Bozek, J. Grilj, M. Guehr, L. J. Frasinski, J. Glownia, D. T. Ha, K. Hoffmann, E. Kukk, B. K. McFarland, C. Miron, E. Sistrunk, R. J. Squibb, K. Ueda, R. Santra, and N. Berrah, Nature Comm. **5**, 4281 (2014).